Acta Pharmaceutica Sinica B 2021;11(1):271−282

Chinese Pharmaceutical Association
Institute of Materia Medica, Chinese Academy of Medical Sciences

Acta Pharmaceutica Sinica B

www.elsevier.com/locate/apsb
www.sciencedirect.com

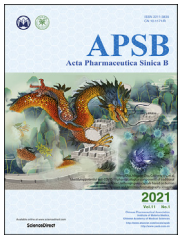

ORIGINAL ARTICLE

Photothermal/matrix metalloproteinase-2 dual-responsive gelatin nanoparticles for breast cancer treatment

Xiaojie Chen[a], Jiafeng Zou[a], Ke Zhang[a], Jingjing Zhu[a], Yue Zhang[a], Zhihong Zhu[a], Hongyue Zheng[b], Fanzhu Li[a,*], Ji-Gang Piao[a,*]

[a]*College of Pharmaceutical Sciences, Zhejiang Chinese Medical University, Hangzhou 310053, China*
[b]*Libraries of Zhejiang Chinese Medical University, Zhejiang Chinese Medical University, Hangzhou 310053, China*

Received 23 June 2020; received in revised form 7 August 2020; accepted 11 August 2020

KEY WORDS

Breast cancer;
Gelatin;
Indocyanine green;
Doxorubicin;
Nanoparticle;
Size-variable;
Chemo−photothermal therapy;
MMP-2

Abstract The chemotherapy combined with photothermal therapy has been a favorable approach for the treatment of breast cancer. In present study, nanoparticles with the characteristics of photothermal/matrix metalloproteinase-2 (MMP-2) dual-responsive, tumor targeting, and size-variability were designed for enhancing the antitumor efficacy and achieving "on-demand" drug release markedly. Based on the thermal sensitivity of gelatin, we designed a size-variable gelatin nanoparticle (GNP) to encapsulate indocyanine green (ICG) and doxorubicin (DOX). Under an 808 nm laser irradiation, GNP-DOX/ICG responded photothermally and swelled in size from 71.58 ± 4.28 to 160.80 ± 9.51 nm, which was beneficial for particle retention in the tumor sites and release of the loaded therapeutics. Additionally, GNP-DOX/ICG showed a size reduction of the particles to 33.24 ± 4.11 nm and further improved drug release with the degradation of overexpressed MMP-2 in tumor. In the subsequently performed *in vitro* experiments, it was confirmed that GNP-DOX/ICG could provide a therapeutic effect that was enhanced and synergistic. Consequently, GNP-DOX/ICG could efficiently suppress the growth of 4T1 tumor *in vivo*. In conclusion, this study may provide a promising strategy in the rational design of drug delivery nanosystems based on gelatin for chemo-photothermal therapy to achieve synergistically enhanced therapeutic efficacy against breast cancer.

*Corresponding authors.
E-mail addresses: lifanzhu@zcmu.edu.cn (Fanzhu Li), jgpiao@zcmu.edu.cn (Ji-Gang Piao).

Peer review under responsibility of Chinese Pharmaceutical Association and Institute of Materia Medica, Chinese Academy of Medical Sciences.

https://doi.org/10.1016/j.apsb.2020.08.009

1. Introduction

Breast cancer is one of the malignant tumor, following lung cancer in 2018[1], which has attracted tremendous attentions[2]. Currently, clinical methods have been used for breast cancer treatment such as surgery, chemotherapy, radiotherapy, and immunotherapy[3,4]. However, while chemotherapy has been shown to be an efficient treatment for breast cancer patients after surgery, it is limited by low therapeutic and targeting efficacy and high non-discriminable system toxicity[5]. Hence, it is necessary to develop a more efficient and less toxic therapy to overcome these disadvantages.

Photothermal therapy (PTT) is a spatiotemporally controlled and non-invasive treatment for cancer[6]. PTT utilizes photothermal agents, *e.g.*, gold nanostructures[7−18], carbon nanostructures[19−26], conjugated polymers[27−31], and indocyanine green (ICG) containing carriers[32−34], to transform near-infrared (NIR) laser rays into rapid, localized heating to cause irreversible damage and ablate cancer cells. Numerous researches have reported that PTT has abilities to increase cellular uptake of drugs, overcome drug resistance, lower the side effects and increase the anticancer efficacy of chemotherapeutics[35−39]. Thus, integrating photothermal and chemo-based therapies into one nanoplatform to achieve combinational therapy and synergistic therapeutic effect has acquired tremendous interest[40,41]. However, non-degradable components and sophisticated engineering processes for the fabrication of such particles may limit their potential clinical translation. Therefore, it is urgent to develop drug delivery nanosystems with excellent biocompatibility and at the same time ease of preparation.

ICG is a U.S. Food and Drug Administration (FDA)-approved and clinically used NIR dye. It has received extensive attention in fluorescence imaging and PTT applications[32,37,42], but is limited by easy photobleaching and fast body clearance[43,44]. Doxorubicin (DOX) is an efficient therapeutic in cancer therapy, however, it suffers from severe side effects, including cardiotoxicity, bone marrow suppression, and multidrug resistance[45]. Hence, it is necessary for us to search a novel delivery nanosystem to reduce toxicity, prolong the permeation and retention of drugs in tumor tissues, and enhance the antitumor efficacy.

To this end, several tumor microenvironment stimuli-responsive nanoparticles have been constructed, which could be triggered by acidic pH, overexpressed enzymes, and other pathological stimuli[46]. As we all know, particle size is the key factor in tumor accumulation and retention[47]. Small nanoparticles generally show stronger tumor permeability than large nanoparticles, but are limited by poor circulating half-life time and tissue distribution; large nanoparticles display enhanced tumor retention and prolonged blood circulation[48]. Hence, constructing size changeable nanoparticles could not only facilitate their accumulation in tumor tissue, but also improve their tumor retention, without causing any side effects to normal tissues[49]. Su et al.[50] designed a size changeable graphene quantum dot nanoaircraft for enhanced penetration and delivery of DOX deep into tumor tissue, which was triggered by pathological pH. Xu et al.[51] constructed an enzyme-responsive gelatin-coated nanoparticle, which could be degraded by overexpressed matrix metalloproteinase-9 (MMP-9) in tumor tissues, exhibiting less cytotoxicity to normal cells and effective antitumor efficacy. However, these stimuli-responsive nanoparticles are limited by their complicated synthetic processes and restricted availability. Taking into account of these problems, designing microenvironment stimuli-responsive nanoparticles with simple synthesis, low cost and favorable biodegradability may be a promising strategy.

Gelatin is a natural polymer derived from the partial hydrolysis of collagen that has a number of outstanding properties, including low cost, biocompatibility, and biodegradability[52−54]. Furthermore, gelatin is approved by the FDA as Generally Regarded as Safe material[55]. Gelatin is known as a natural thermo-reversible hydrogel due to its strong intermolecular hydrogen bonds. At temperatures above 40 °C, the hydrogen bonds break and gelatin molecules disassemble[56,57]. Moreover, gelatin can be degraded by matrix metalloproteinase-2 (MMP-2) into its sub-compounds, which is 5−7-fold overexpressed in most cancer microenvironments as compared to normal tissues[58,59]. These properties make gelatin an ideal candidate as an integrative nanoplatform for photothermal and chemotherapy treatments[57].

To solve the problems of biocompatibility, scalable manufacturing for industry and high cost of size changeable nanoparticles[46], several gelatin nanoparticles have been designed to deliver drugs. Hu et al.[60] proposed an MMP-2 sensitive gelatin nanoparticle, which showed size-reduction property and excellent tumor targeting and penetration. Ruan et al.[61] constructed gelatin-coated nanoparticles, which could be degraded by MMP-2 and facilitate small-sized nanoparticles better penetration into glioma.

Encouraged by the outstanding properties of gelatin, we have constructed a photothermal/MMP-2 dual-responsive nanosystem to achieve "on-demand" drug release and synergistic therapeutic efficacy. Hence, gelatin nanoparticles (GNP-DOX/ICG) were designed to co-encapsulate a photothermal agent (ICG) and chemotherapeutic (DOX). A commonly used crosslinker, glutaraldehyde (GA), was added to provide higher mechanical properties and improved stability[54,62,63]. Upon laser irradiation, GNP-DOX/ICG swelled, remained in the tumor sites, and released its payloads of ICG and DOX. GNP-DOX/ICG was then degraded by MMP-2, and released DOX and ICG to further penetrate into tumors. Such nanoparticles can obviously increase the efficacy of anticancer therapeutics.

2. Materials and methods

2.1. Materials

Doxorubicin hydrochloride (DOX·HCl) was obtained from Shanghai Yuanye Biological Technology Co., Ltd. (Shanghai, China). 3-(4,5-Dimethylthiazol-2-yl)-2,5-diphenyltetrazolium bromide (MTT), type-A gelatin (99%) and indocyanine green (ICG) were obtained from Sigma−Aldrich (St. Louis, MO, USA). The glutaraldehyde solution (25% water solution) was purchased from Shanghai Lingfeng Chemical Reagent Co., Ltd. (Shanghai, China). The active human recombinant MMP-2 was purchased from EMD Chemicals (Shanghai, China). 4T1 cells were purchased from Cell Bank of Chinese Academy of Sciences (Shanghai, China). Female BALB/c mice (5−6 weeks, 20 ± 2 g) were purchased from the laboratory animal center of Zhejiang Chinese Medical University [SYXK (Zhe) 2018-0012, Hangzhou, China]. All animal experiments were performed in conformity with the guidelines approved by the Animal Experimentation Ethics Committee of Zhejiang Chinese Medical University, Hangzhou, China.

2.2. Preparation of GNP-DOX/ICG with different degrees of crosslinking

Gelatin nanoparticles (GNP) were performed according to a method previously reported with some modications[64]. Acetone (25 mL) was mixed with gelatin solution (25 mL and 0.05 g/mL) under the temperature of 50 °C, and stirred gently for 2 min. After discarding the supernatant, the precipitated gel was then dissolved at 50 °C in 25 mL of water containing ICG (10 mg) and DOX (40 mg). Then hydrochloric acid was used to adjust the pH to 3. During a 25-min period, acetone (75 mL) was added to the mixture with continuous stirring under 40 °C. Different concentrations (0, 50 and 200 μL) of 1% glutaraldehyde were then added to crosslink the gelatin for 2 h. Finally, the free ICG, DOX, and glutaraldehyde were removed by repeated centrifugation (3000 rpm, 10 min, and three times; 5810R, Eppendorf, Hamburg, Germany) and resuspended with 20 mL water. The GNP-DOX or GNP-ICG was prepared without ICG or DOX while keeping the other conditions the same.

2.3. Characterization of GNP-DOX/ICG

Using dynamic light scattering (DLS; Malvern Nano-ZS90, Worcestershire, UK), the hydrodynamic diameter as well as zeta potential of GNP-DOX/ICG treated with or without an 808 nm irradiation under the density of 1 W/cm^2 for 10 min and MMP-2 (1 μg/mL, 12 h) were characterized. The morphological features were imaged *via* transmission electron microscopy (TEM; H-7650, Hitachi, Tokyo, Japan). Using a UV−Vis spectrometer (SpectraMax M2, Molecular Devices, Sunnyvale, CA, USA), the UV−Vis NIR absorption spectra of GNP-DOX/ICG in phosphate-buffered saline (PBS) was recorded.

2.4. Drug loading and encapsulation efficiency

ICG and DOX drug loading (DL) yields and encapsulation efficiency (EE) within the GNP were determined by measuring ICG absorbance at 800 nm and DOX fluorescence intensity at 595 nm (λ_{ex} = 488 nm) and comparing them to standard curves of the free ICG and DOX. Briefly, the standard curve of ICG in PBS was obtained by measuring the absorbance at 800 nm in solutions of free ICG at different concentrations with a UV−Vis spectrometer (Molecular Devices). The standard curve of DOX in PBS was obtained by measuring the emission fluorescence at 595 nm for different DOX concentrations with a fluorimeter (F-4600 spectrofluorometer, Hitachi, Tokyo, Japan). The DL and EE were calculated based on Eqs. (1) and (2), respectively:

$$\mathrm{DL}\ (\%) = \frac{\text{Weight of loaded drug}}{\text{Total weight of GNP} - \text{DOX/ICG}} \times 100 \quad (1)$$

$$\mathrm{EE}\ (\%) = \frac{\text{Weight of loaded drug}}{\text{Total weight of feeding drug}} \times 100 \quad (2)$$

2.5. In vitro release

The DOX release profile from the GNP-DOX/ICG with different degrees of crosslinking, with or without an 808 nm laser irradiation at the density of 1 W/cm^2 for 10 min and MMP-2 (1 μg/mL) was measured through a dialysis method. Briefly, GNP-DOX/ICG (DOX: 300 μg) was first suspended into a dialysis bag (1500 Da) and then placed into 50 mL of PBS (pH 7.4). The release experiment was conducted at the temperature of 37 °C with constant shaking. To study the effect of ICG-induced photothermal effect on DOX release, GNP-DOX/ICG was dealt with laser irradiation and/or MMP-2. At selected time intervals (15, 30, 60, 120, 130, 180, 240, 250, 300, and 360 min), aliquots of the solution out of the dialysis bag were collected, following which the release amounts of DOX were obtained using a fluorimeter (Hitachi).

2.6. In vitro photothermal characterizations

To characterize the photothermal transformation of GNP-DOX/ICG, the temperature rising in its dispersion (ICG concentration of 5−40 μg/mL and 1 mL in PBS) was monitored during 5 min irradiation of 808 nm laser with a power density of 1 W/cm^2.

2.7. In vitro cytotoxicity evaluation

The cytotoxicity of GNP or GNP-DOX/ICG on 4T1 cells was determined through MTT method. 4T1 cells (1×10^4 cells per well) were seeded in 96-well plate and incubated at a constant temperature incubator (ThermoFisher, Waltham, MA, USA). Once confluence reached 80%, the culture medium was replaced with fresh medium comprising different concentrations of free GNP with different degrees of crosslinking (concentrations: 1−256 μg/mL) and GNP-DOX/ICG (DOX concentrations: 10−40 μg/mL). After 4-h incubation, GNP-DOX/ICG + laser group was treated with 5 min irradiation by an 808 nm laser with the density of 1 W/cm^2. After another 20-h incubation, 20 μL MTT (5 mg/mL) was added for another 4-h incubation. Then 150 μL DMSO was used to replace MTT solution. The absorbance value at 490 nm was determined by monitoring the optical densities with a microplate reader (Synergy TM2, BIOTEK, Winooski, VT, USA).

2.8. In vitro cellular uptake

To evaluate GNP-DOX/ICG cellular uptake at different conditions, 1×10^5 4T1 cells were seeded in a 12-well plate and incubated at 37 °C overnight. Once the confluence reached 80%, the culture medium was replaced with a fresh medium that containing GNP-DOX/ICG (DOX concentration of 20 μg/mL) for 12 h. As for the group of laser irradiation, the cells were irradiated using an 808 nm laser at the density of 1 W/cm^2 for 5 min after incubated 3 h. After another 9-h incubation followed by DAPI staining and PBS washing, GNP-DOX/ICG intracellular localization in 4T1 cells was determined using a laser scanning confocal microscope (Olympus, Tokyo, Japan).

2.9. In vivo imaging and biodistribution analysis

Once tumor volumes reached 100−200 mm^3, the tumor-bearing BALB/c mice were randomly divided into two groups. Then 200 μL of PBS or GNP-DOX/ICG (ICG concentration: 1 mg/mL) was intravenously injected into mice. The fluorescence signal of ICG was acquired at 0, 0.5, 1, 2, 4, 8, 12, and 24 h after the injection through an *in vivo* imaging system (excitation: 704 nm and filter: 735 nm). At 24 h after the injection, mice were sacrificed. And their major tissues including heart, liver, spleen, lung and kidney, and tumor were collected for *ex vivo* imaging. Then the

major tissues and tumor were fixed in 10% paraformaldehyde and prepared into tissue slices. The fluorescence distribution of tissue slices was determined by a laser scanning confocal microscope.

In order to compare the retention of GNP-DOX/ICG with or without laser irradiation, one group of mice treated with GNP-DOX/ICG were irradiated by an 808 nm laser at the density of 1 W/cm^2 for 10 min after injected for 24 h. Then the fluorescence signals of ICG were acquired at different days *via* an *in vivo* imaging system.

2.10. *In vivo photothermal characterizations*

Six 4T1 tumor-bearing BALB/c mice were divided into two groups. Then 200 μL of PBS control or GNP-DOX/ICG (ICG concentration: 1 mg/mL) were intravenously injected into mice. At 24 h following the injection, the tumor sites of all mice groups were irradiated by using an 808 nm laser at the density of 1 W/cm^2 for 5 min. The temperature change in the tumor was determined by recoding its thermographs using an infrared thermal camera (ICI 7320, Infrared Camera Inc., Beaumont, TX, USA).

2.11. *In vivo antitumor evaluation*

Once tumor volumes reached approximately 100−200 mm^3, thirty 4T1 tumor-bearing BALB/c mice were randomly divided into six groups. Among these mice groups, two groups were intravenously injected with 200 μL PBS or GNP-DOX, respectively. And the other four groups were injected with 200 μL of GNP-ICG or GNP-DOX/ICG (ICG concentration: 1 mg/mL) *via* the tail vein, respectively. For the laser irradiated groups, tumor irradiation was performed for 10 min using an 808 nm laser at 1 W/cm^2 after intravenous injected for 24 h. The NIR irradiation was repeated once daily and over a span of 21 days thereafter. The tumor volume, body weight, and survival ratio of the mice were recorded every other day. The tumor volume was calculated according to Eq. (3):

$$V = \text{Tumor length} \times \text{Tumorwidth}^2/2 \quad (3)$$

2.12. *Histopathology analysis*

After 21 days, the mice were sacrificed, and the major organs and tumors were collected and fixed in 10% paraformaldehyde. After that, the tissues were stained with hematoxylin and eosin (H&E) and terminal-deoxynucleotidyl transferase mediated nick end labeling (TUNEL) according to the protocol from manufacturer. Then an optical microscope (AXIO SCOPE.A1, Zeiss, Jena, Germany) was used to evaluate each organ's tissue damage and cell apoptosis of the tumor tissue, respectively.

2.13. *Statistical analysis*

All data are presented as mean or mean ± standard deviation. Statistical significance was determined *via* SPSS 23. $P < 0.05$ indicated a statistical difference, and a statistically significant difference was indicated by $P < 0.01$.

3. Results and discussions

As depicted in Fig. 1, GNP-DOX/ICG was fabricated using a two-step desolvation method with ICG and DOX loadings. Different concentration of glutaraldehyde was used as a crosslinker to provide higher mechanical properties, improve stability, and modulate subsequent responsive drug release kinetics. GNP-DOX/ICG is capable of responsively releasing the payloads of ICG and DOX through photothermal actuation and MMP-2 degradation-induced, partial dissolution and disassembly of gelatin molecules to achieve synergistic effects in photothermal and chemotherapy treatments.

3.1. *Characterization of GNP-DOX/ICG*

GNP-DOX/ICG with different crosslinking degrees were characterized with UV−Vis. Each sample displayed characteristic peaks of UV−Vis absorption at 480 nm for DOX and 777 nm for ICG, which indicated that DOX and ICG were successfully encapsulated into the nanoparticles (Fig. 2A). Based on DLS result (Fig. 2B), the size of non-, low-, and high-crosslinked GNP-DOX/ICG were 83.40 ± 5.15, 71.58 ± 4.28, and 67.80 ± 6.22 nm, respectively. These results indicate that the addition of crosslinkers leads to a more compact nanostructure and smaller size in the nanoparticles. A smaller size can facilitate GNP-DOX/ICG accumulation at the tumor site and largely decrease their diffusional hinderance[65]. In addition, all the nanoparticles displayed similar negative surface charges, which may reduce non-specific interactions with proteins in the blood and prolong their circulation time. The DL of DOX and ICG within GNP-DOX/ICG with different crosslinking degrees were monitored next using a spectrometer and fluorimeter as this is important for their biomedical applications[32]. The DOX DLs of non-, low-, and high-crosslinked GNP-DOX/ICG were 2.13 ± 0.12%, 5.17 ± 0.29%, and 8.23 ± 0.68%, respectively. The ICG DLs were calculated to be 5.42 ± 0.31%, 7.27 ± 0.66%, and 10.12 ± 0.12%, respectively (Fig. 2C). The DOX EEs of non-, low-, and high-crosslinked GNP-DOX/ICG were 4.52 ± 0.25%, 11.35 ± 0.60%, 18.68 ± 1.42%, respectively. The ICG EEs were 47.78 ± 2.63%, 65.32 ± 1.31%, 78.86 ± 1.01%, respectively. It should be noted that the addition of crosslinker led to higher loading of both DOX and ICG, which should be attributed to improved stability. For evaluating the photothermal potency of GNP-DOX/ICG, their temperature changes were monitored by using an thermal imaging camera under laser irradiation (Fig. 2D). After irradiated for 5 min using an 808 nm laser at 1 W/cm^2, GNP-DOX/ICG exhibited temperature rise profiles at various concentrations of ICG. The results implied that the photothermal effect was concentration dependent. At 40 μg/mL of ICG, GNP-DOX/ICG was increased by 36.1 °C at 300 s with laser irradiation. Meanwhile, at 5 μg/mL of ICG, the temperature was elevated by 9.5 °C with irradiation for 300 s. Based on normal body temperature of 37 °C, such a variation of GNP-DOX/ICG with ICG as low as 5 μg/mL could increase the temperature above 46 °C and hence lead to irreversible damage to tumor cells[65].

It has been reported that gelatin is a natural thermo-reversible hydrogel due to its strong intermolecular hydrogen bonds. At temperature above 40 °C, the hydrogen bonds break and gelatin

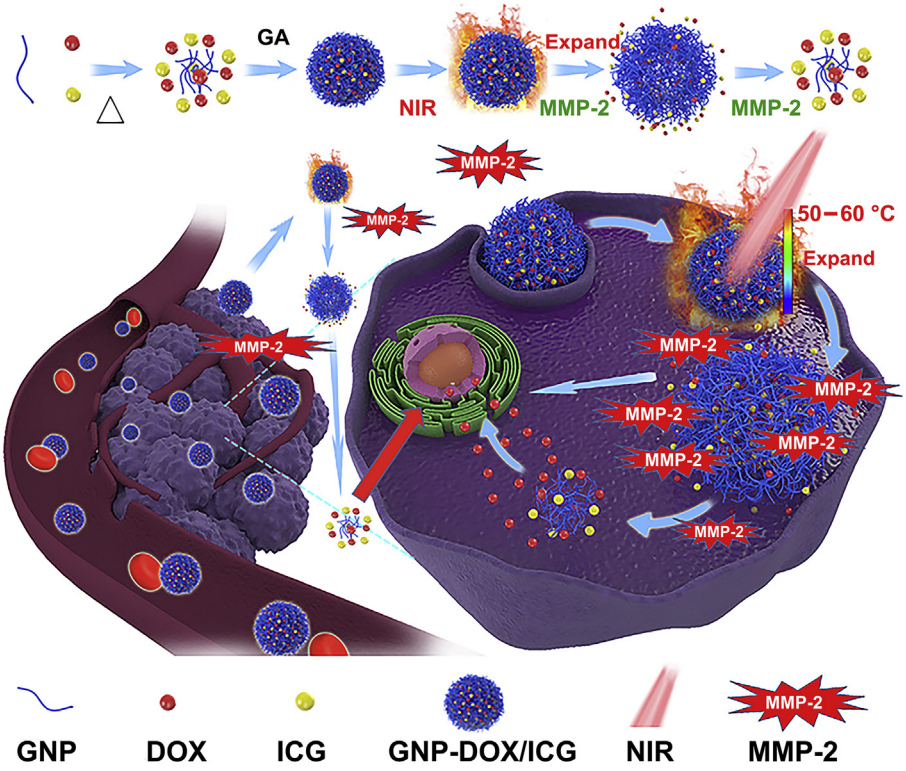

Figure 1 Schematic illustration for GNP-DOX/ICG preparation and subsequent blood circulation, cellular uptake, and responsive drug release enabled by laser irradiation and MMP-2 degradation.

molecules disassemble and switch to a solution state, during which it would experience a swelling process[57]. Pal et al.[55] have shown that the swelling ratio of gelatin nanoparticles increased from room temperature to 37 °C and thereafter decreased over 37 °C, which was attributed to the improvement of the kinetic energy of water molecules entrance and the breakage of binding forces between water molecules and gelatin molecules, respectively.

TEM was applied to monitor the morphology transition of GNP-DOX/ICG treated with or without laser irradiation and MMP-2 incubation. As shown in Fig. 3A, non-, low-, and high-crosslinked GNP-DOX/ICG displayed spherical nanostructures. After laser irradiation, non-crosslinked GNP-DOX/ICG displayed a hollow nanocapsule morphology as their hydrodynamic diameter increased from 83.40 ± 5.15 to 210.60 ± 11.35 nm (Fig. 3B), which indicated that the photothermal effect led to volumetric expansion of the nanoparticles based on the insoluble–soluble transformation of gelatin molecules. This phenomenon could be explained that the hydrogen bonds of gelatin in GNP-DOX/ICG collapsed partially with the increase of temperature; then the gelatin became more flexible, presenting a higher swelling capacity[66]. Hence, with the increasing temperature caused by NIR laser irradiation, GNP-DOX/ICG exhibited a swelling process reflected by the size increase.

Meanwhile, the degrees of crosslinking with glutaraldehyde also had an important affection in the potency of laser and MMP-2[67]. Compared to non-crosslinked GNP-DOX/ICG, low-crosslinked GNP-DOX/ICG exhibited lower volumetric expansion (71.58 ± 4.28 to 160.80 ± 9.51 nm). The high-crosslinked GNP-DOX/ICG exhibited a less significant change after laser irradiation (67.80 ± 6.22 to 115.80 ± 7.25 nm). Furthermore, with the combination treatment of laser irradiation and MMP-2, all three GNP-DOX/ICG were degraded and their particle sizes notably decreased to 20.58 ± 3.20, 33.24 ± 4.11, and 50.11 ± 4.25, respectively (Fig. 3B). And the order of laser and MMP-2 has little effects on hydrodynamic diameter of different-crosslinked GNP-DOX/ICG (Supporting Information Fig. S1). Results from TEM and DLS suggest that GNP-DOX/ICG with different crosslinking degrees can lead to the transformation of small–large–small as a response to laser irradiation and MMP-2, thereby facilitating drug penetration into the core area at tumor sites. GA is the most widely-used crosslinker in providing higher mechanical properties and improving stability of gelatin. As a protein molecule, gelatin could react with the aldehyde groups in GA by using the available free amine groups[68]. Hence, with the increasing of glutaraldehyde, the size of nanoparticles exhibited a consistent decrease[55]. And with the addition of MMP-2, the gelatin in GNP-DOX/ICG would be degraded, and need to overcome the crosslink strength with GA in the meantime.

The cumulative drug release from GNP-DOX/ICG with or without laser irradiation or MMP-2 was determined through a dialysis method (Fig. 3C). Few DOX was released when the three

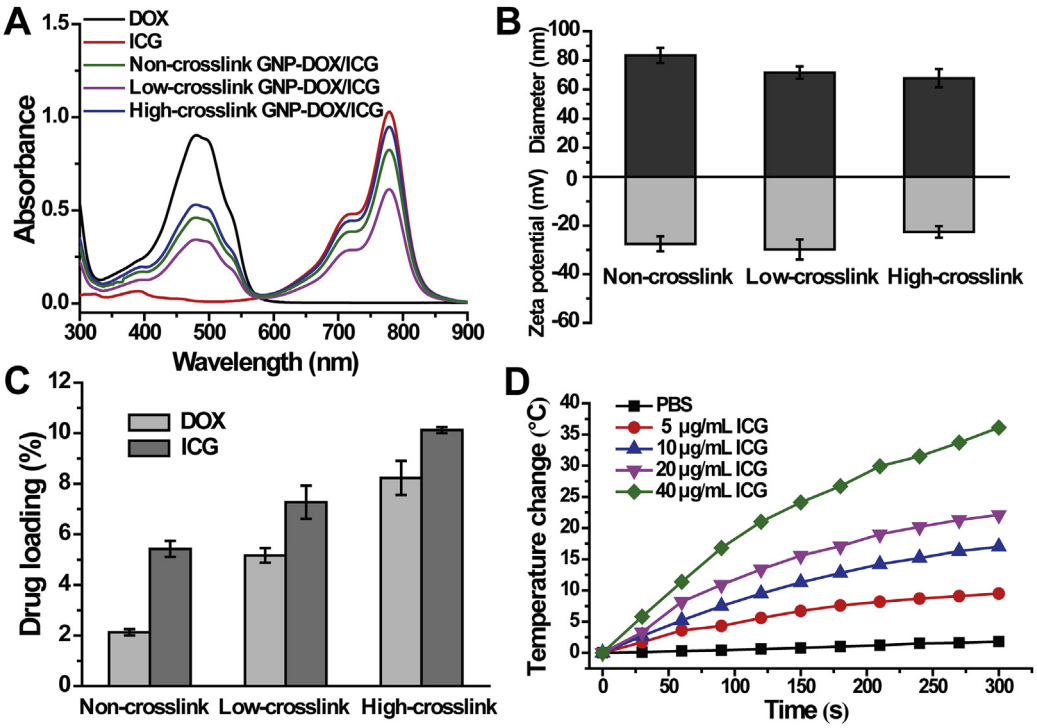

Figure 2 Characterization for nanoparticles with different crosslinking degrees: (A) UV−Vis absorption spectra of DOX, ICG, and GNP-DOX/ICG. (B) Zeta potential and hydrodynamic diameter of GNP-DOX/ICG. Data are presented as mean or mean ± SD ($n = 3$). (C) Drug loading yields of GNP-DOX/ICG. Data are presented as mean or mean ± SD ($n = 3$). (D) The temperature changes in GNP-DOX/ICG dispersions in PBS (ICG concentration of 5, 10, 20, and 40 μg/mL) when irradiated with 808 nm laser at a power density of 1 W/cm^2 for 5 min.

groups were dialyzed against PBS. After irradiation for 10 min, non- and low-crosslinked GNP-DOX/ICG exhibited laser-dependent release properties, and approximately 47.4% and 35.7% were respectively released after 6 h. With a combination of laser irradiation and MMP-2, non- and low-crosslinked GNP-DOX/ICG exhibited a higher cumulative drug release of 57.3% and 44.8%, respectively. In comparison, the DOX release of high-crosslinked GNP-DOX/ICG did not obviously increase. And these results correlated with the results from DLS and TEM (Fig. 3A and B). Considering the parameters involved in DL, stability, and responsive drug release behavior, the low-crosslinked GNP-DOX/ICG was selected for the subsequent *in vivo* and *in vitro* antitumor evaluation.

3.2. *In vitro cytotoxicity evaluation*

The cytotoxicity of blank GNP and GNP-DOX/ICG, and photothermal effect of ICG against 4T1 cells were evaluated by MTT assay. Almost no toxicity was observed after incubating 4T1 cells with GNP with different crosslinking degrees (Fig. 4A), indicating excellent biocompatibility of GNP. Meanwhile, 4T1 cells survival rates were dramatically reduced with an increase of DOX concentration in the nanoparticles (Fig. 4B). With the combination of laser, cell survival rate of GNP-DOX/ICG (DOX: 40 μg/mL) was further reduced to below 20%, indicating that laser irradiation has an effective lethality on tumor cells.

3.3. *In vitro cellular uptake and intracellular distribution*

Targeted delivery to specific cells is crucial for cancer therapy. The intracellular delivery of nanosystems could be enhanced *via* photothermal effect on account of increased cell membrane permeability and improved endocytosis[67,69]. The cellular uptake of GNP-DOX/ICG was evaluated by confocal laser scanning microscopy for monitoring cellular targeting efficiency. DOX could exert its therapeutic effects in the nucleus because of its quick intercalation as well as excellent bonding ability with DNA[70]. In GNP-DOX/ICG treated cells, a red fluorescence was from DOX, and the blue fluorescence was the nucleus stained with DAPI. As displayed in Fig. 4C, GNP-DOX/ICG-treated groups exhibited DOX fluorescence that was mainly distributed at the cell surface and cytoplasm, while a little fluorescence can be seen in the nucleus. However, with laser treatment, more DOX distributed within the cytoplasm and a higher red fluorescence could be seen in the nucleus. This suggests that the laser treatment can be used to facilitate the entrance of drugs into cells, followed by responsive drug release.

3.4. *In vivo imaging and biodistribution analysis*

The inherent and sensitive fluorescence of ICG was used to measure the amounts of accumulated GNP-DOX/ICG in the tumor and different organs, without the need for additional radio or

fluorescent labeling[32]. To evaluate the real-time biodistribution of GNP-DOX/ICG, an imaging system was used to *in vivo* image at different time intervals. Fig. 5A illustrated the ICG FL signal and intensity distribution of GNP-DOX/ICG. ICG FL could be visualized in the GNP-DOX/ICG treated group at 24 h postinjection, indicating that GNP-DOX/ICG could achieve prolonged circulation. This is most likely due to the protection provided by gelatin. Interestingly, the ICG FL signal of GNP-DOX/ICG reached a peak at 1 h postinjection in the tumor site, decreased, increased again at 12 h. The highest level of fluorescent was at 24 h postinjection, which demonstrated the increased tumor targeting efficiency. The distribution of GNP-DOX/ICG in the major organs and the tumor was displayed in Fig. 5B and C. The results showed that ICG mostly accumulated in the liver, followed by the spleen, lung, kidney, and tumor. The ICG signal in spleen and lung might be due to the effects of reticuloendothelial system (RES). Generally, a large amount of nanoparticles accumulated in the RES-associated organs such as liver, lung and spleen after administration, which will result in a low percentage (~5%) retained in the tumor site, and then possibly followed by excretion in feces or recirculation[71,72]. As shown in Supporting Information Fig. S4, tissue slices were used to further elucidate the fluorescent distribution after treated with GNP-DOX/ICG, which were consistent with the results of *in vivo* imaging and biodistribution analysis.

In order to compare the fluorescence changes with or without laser irradiation, the ICG FL signals were recorded by imaging system. As shown in Fig. 5D and E, the FL signals of GNP-DOX/ICG around the tumor site under laser irradiation were much higher than the group without laser irradiation. These phenomena could be due to both the laser-induced thermoresponsive behavior and the retention caused by gelatin swelling.

3.5. *In vivo photothermal characterizations*

Owing to sufficient tumor uptake, GNP-DOX/ICG could generate rapid local heating upon laser irradiation. At 24 h after GNP-DOX/ICG injection (200 μL and ICG concentration of 1 mg/mL), the photothermal effect at tumor site was measured *via* an infrared thermal camera while being irradiated. Simultaneously, the conditions of irradiation were laser wavelength of 808 nm and a

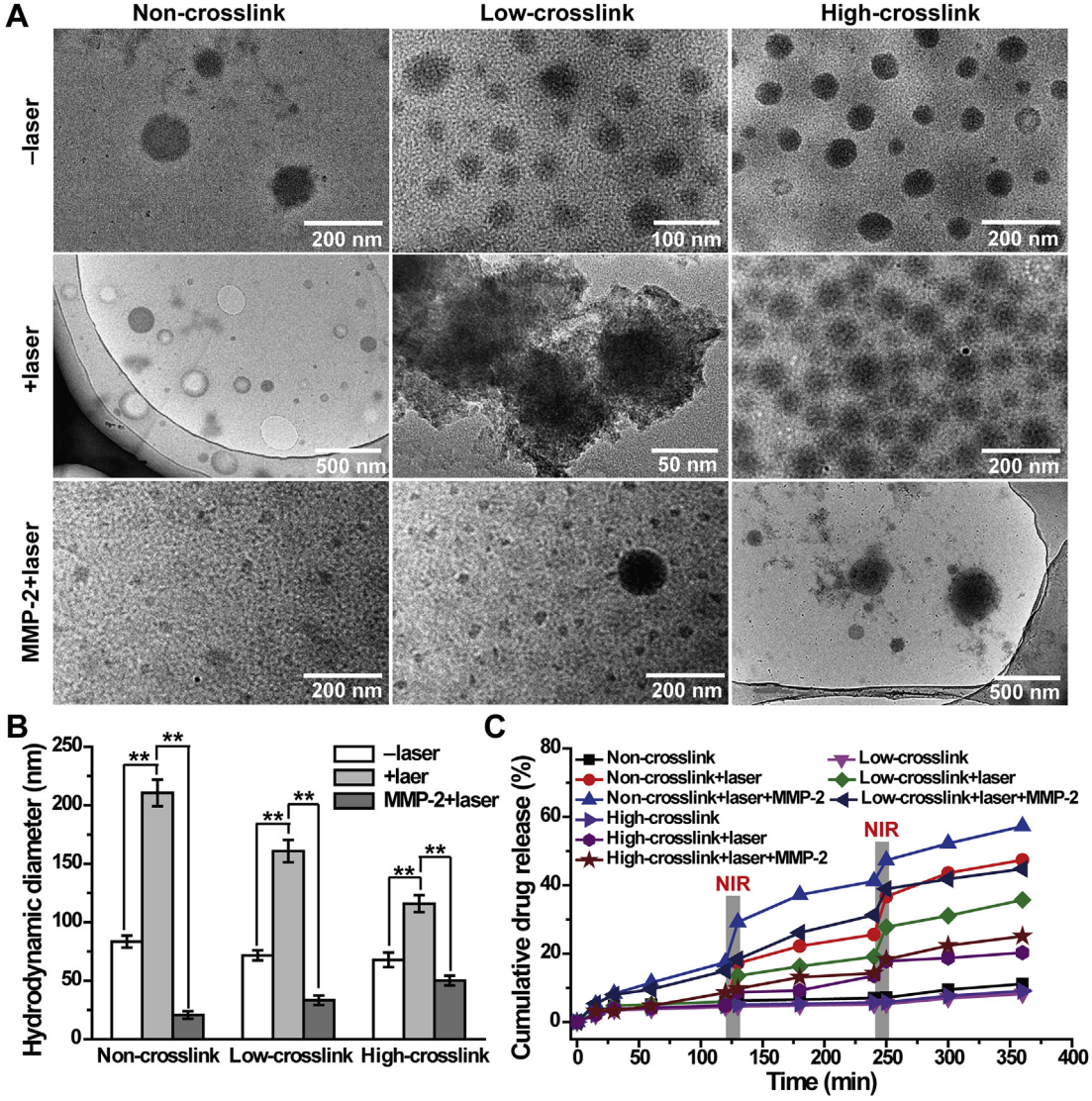

Figure 3 (A) TEM images, (B) hydrodynamic diameter, and (C) cumulative drug release of non-, low-, and high-crosslinked GNP-DOX/ICG treated with or without laser irradiation and MMP-2 incubation. Data are expressed as means ± SD ($n = 3$). $^{**}P < 0.01$.

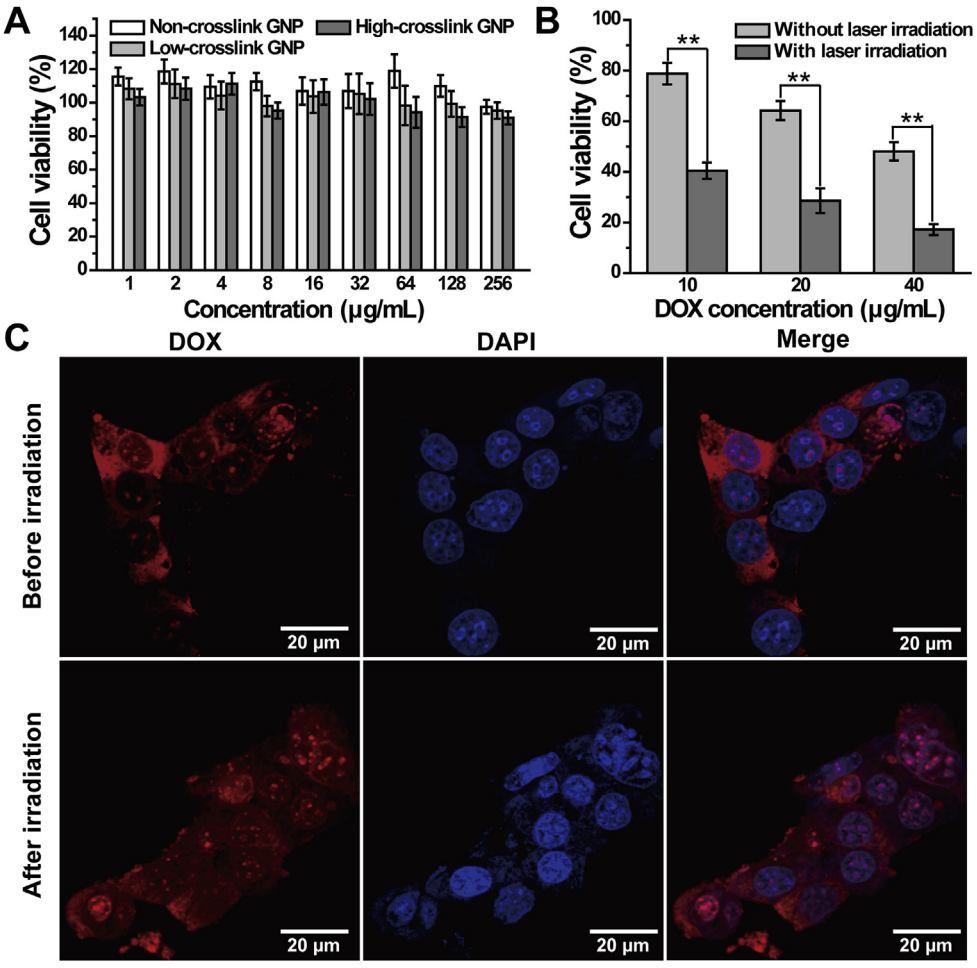

Figure 4 (A) The viability of 4T1 cells treated with GNP of varying concentrations. (B) The viability of 4T1 cells after treatment with GNP-DOX/ICG containing various DOX concentrations with or without NIR laser irradiation (808 nm, 1 W/cm^2, and 5 min). (C) Confocal laser scanning microscopy images of DOX in 4T1 cells treated with GNP-DOX/ICG after 4 h incubation with or without laser irradiation. Data are expressed as means ± SD ($n = 3$). $^{**}P < 0.01$.

power density of 1 W/cm^2. The 5 min laser irradiation increased tumor temperature to 55.9 °C in the GNP-DOX/ICG-treated group, whereas PBS-treated and laser irradiated tumors exhibited no significant increase in temperature (Fig. 5F and G).

3.6. *In vivo antitumor evaluation*

To assess the antitumor effect of combined effect of photothermal and chemotherapy treatment mediated by GNP-DOX/ICG, *in vivo* antitumor evaluation was evaluated in 4T1 tumor-bearing mice. Thirty mice were randomly divided into six groups, and treated with PBS, GNP-DOX, GNP-ICG, GNP-ICG + laser, GNP-DOX/ICG, or GNP-DOX/ICG + laser. The therapeutic efficacy was monitored *via* tumor volume and body weight as well as survival ratio. During the 21-day treating period, the average tumor volume of GNP-ICG + laser and GNP-DOX/ICG + laser-treated mice continuously decreased and remained negligible from Days 13 and 9, respectively (Fig. 6A and D), which mainly were caused by the PTT effect of ICG. However, the average tumor volume of GNP-DOX/ICG-treated mice kept increasing at a slower rate than that of PBS-treated group, which suggested that 4T1 tumors were slightly inhibited by GNP-DOX/ICG. Moreover, results of the mouse survival revealed that mice treated with GNP-ICG + laser and GNP-DOX/ICG + laser achieved 100% survival throughout the 21-day treating period, whereas mice treated with GNP-DOX/ICG and PBS exhibited 20% and 40% loss in survival ratio, respectively (Fig. 6B). The mice treated with GNP-DOX/ICG and PBS led to a slight reduction of body weight, whereas the average body weight treated with GNP-DOX/ICG + laser kept stable (Fig. 6C). Compared to group of single treatment of chemotherapy or PTT, the group of GNP-DOX/ICG + laser-treated mice displayed the best antitumor effect by combining chemotherapy with PTT, indicating the superiority of drug combination.

3.7. *Histopathology analysis*

Whether the GNP-DOX, GNP-ICG and GNP-DOX/ICG groups treated with laser irradiation or not, showed various degrees in

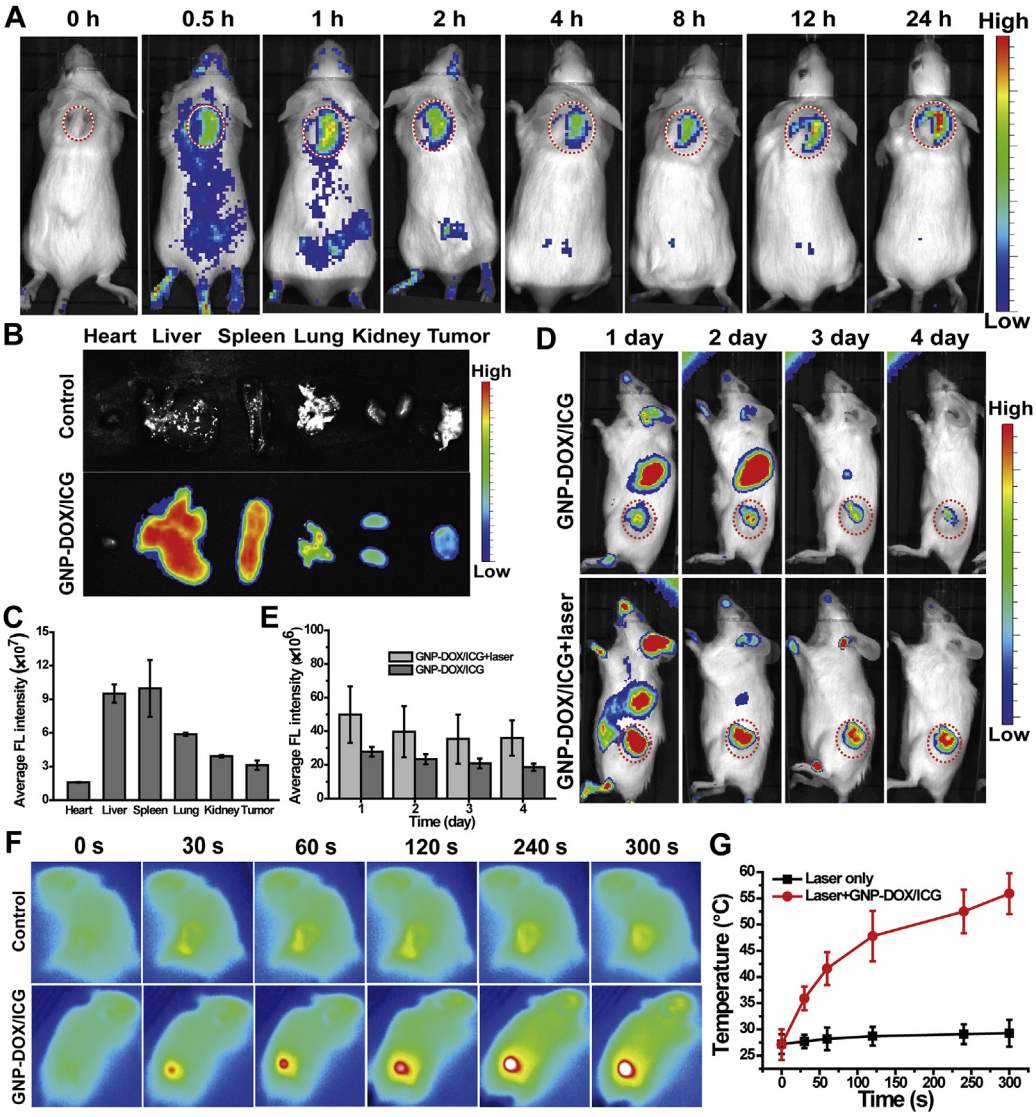

Figure 5 (A) *In vivo* ICG fluorescence images of 4T1 bearing mice following intravenous GNP-DOX/ICG injection at 0, 0.5, 1, 2, 4, 8, 12 and 24 h. (B) *Ex vivo* fluorescence images and (C) fluorescence intensity of major organs and tumors at 24 h following GNP-DOX/ICG injection. Data are presented as mean or mean ± SD ($n = 3$). (D) *In vivo* ICG fluorescence images at different time point. (E) Semi-quantitative analysis of ICG fluorescence intensity around the tumors with or without laser irradiation. Data are presented as mean or mean ± SD ($n = 3$). (F) Near-infrared thermal images and (G) temperature profiles of tumor treated with PBS or GNP-DOX/ICG with an 808 nm laser with a power intensity of 1 W/cm^2. Data are presented as mean or mean ± SD ($n = 3$).

tumor cell necrosis. The GNP-DOX/ICG group with NIR exhibited the largest area of abnormalities or lesions than the PBS-treated mice, which was caused *via* the synergistic effect of DOX and ICG-induced PTT. Furthermore, immunofluorescent TUNEL staining assay was used to evaluate the cell apoptosis of tumors *in vivo* for the chemo−photothermal therapy. The tumor cells in the PBS, GNP-DOX, GNP-ICG and GNP-ICG + laser-treated mice displayed little apoptosis (Fig. 6E and Supporting Information Fig. S3). GNP-DOX/ICG treatment led to a higher tumor cell apoptosis, demonstrating that GNP-DOX/ICG could produce a better chemotherapy effect by enhancing DOX accumulation at the tumor site. Moreover, GNP-DOX/ICG + laser treatment resulted in a significantly increase in the amount of apoptotic and necrotic cells compared to the treatment without laser irradiation. These studies illustrate that chemo−photothermal therapy could efficiently eliminate tumor cells *via* permanent and irreversible DNA/RNA and protein damage[73]. Histological analysis (Supporting Information Fig. S5) of the major organs further indicated that GNP-DOX, GNP-ICG, GNP-ICG + laser and GNP-DOX/ICG treatment did not induce damage to these organs compared with PBS treatment.

4. Conclusions

In this study, we have successfully constructed GNP-DOX/ICG for synergistically delivering DOX and ICG to provide a combination of photothermal and chemo-based therapies. GNP-DOX/ICG exhibited microenvironment-responsive tumor targeting and size-variable capabilities. Most importantly, GNP-DOX/ICG displayed excellent photothermal effects upon irradiated by near-infrared laser, which could obviously improve DOX and ICG cellular uptake within 4T1 cells. Finally, GNP-DOX/ICG showed

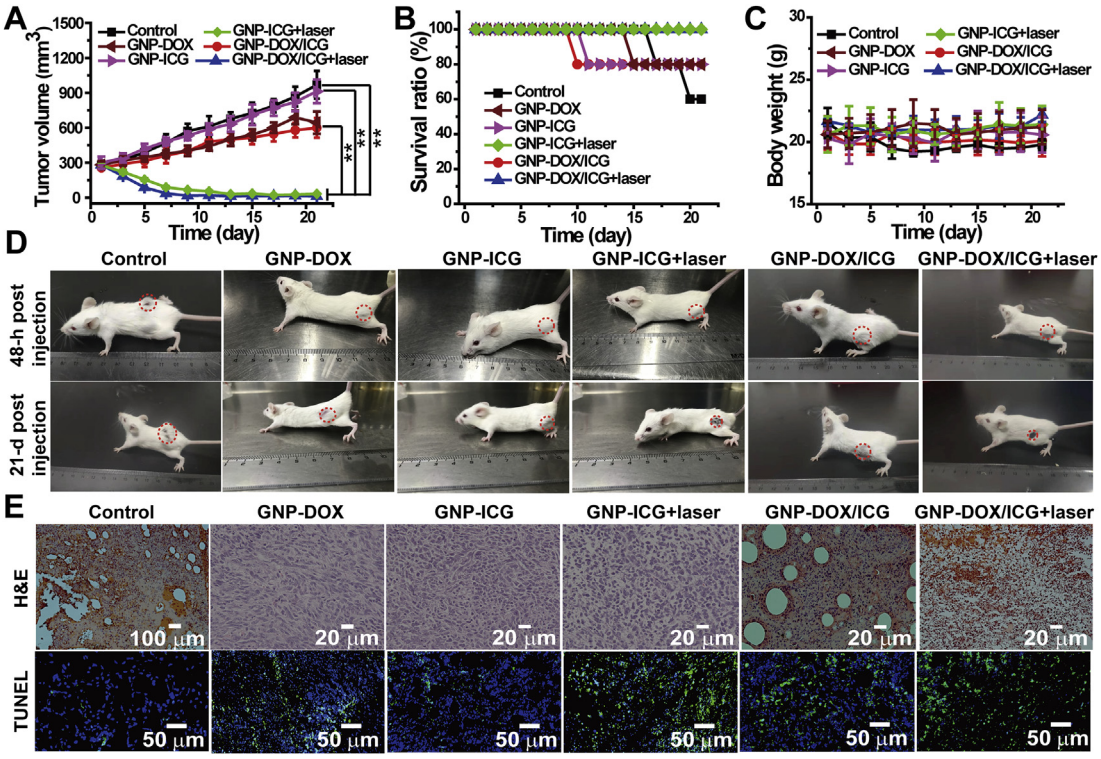

Figure 6 (A) Tumor volume, (B) survival ratio, and (C) body weight alterations treated with PBS, GNP-DOX, GNP-ICG, GNP-ICG + laser, GNP-DOX/ICG, or GNP-DOX/ICG + laser. (D) Photographs of mice at 48 h postinjection and on day 19 after initiating NIR irradiation. (E) H&E staining and TUNEL immunofluorescence of tumors after PBS, GNP-DOX, GNP-ICG, GNP-ICG + laser, GNP-DOX/ICG, and GNP-DOX/ICG + laser treatment. Data are expressed as means ± SD ($n = 5$). $^{**}P < 0.01$.

efficient antitumor effects for breast cancer by combining chemotherapy with PTT. We hold a belief that this work could provide the basis for a promising nanocarrier for the treatment of breast cancer.

Acknowledgments

This work was supported by the National Natural Science Foundation of China (81873014, China), Natural Science Foundation of Zhejiang Province (LQ18E030003, China), China Postdoctoral Science Foundation (2017M621890, China), and the Science and Technology Innovation Team Project of Zhejiang Province (2019R410057, China).

Author contributions

Fanzhu Li and Ji-Gang Piao designed the research. Xiaojie Chen carried out the experiments and performed data analysis. Ke Zhang, Jingjing Zhu and Yue Zhang participated part of the experiments. Zhihong Zhu and Hongyue Zheng provided some suggestions. Xiaojie Chen wrote the manuscript. Jiafeng Zou revised the manuscript. All of the authors have read and approved the final manuscript.

Conflicts of interest

The authors have no conflicts of interest to declare.

Appendix A. Supporting information

Supporting data to this article can be found online at https://doi.org/10.1016/j.apsb.2020.08.009.

References

1. Bray F, Ferlay J, Soerjomataram I, Siegel RL, Torre LA, Jemal A. Global cancer statistics 2018: GLOBOCAN estimates of incidence and mortality worldwide for 36 cancers in 185 countries. *CA Canc J Clin* 2018;**68**:394–424.
2. Liu XR, Wang C, Ma HS, Yu FY, Hu FQ, Yuan H. Water-responsive hybrid nanoparticles codelivering ICG and DOX effectively treat breast cancer *via* hyperthermia-aided DOX functionality and drug penetration. *Adv Healthc Mater* 2019;**8**:1801486.
3. Wan GY, Chen BW, Li L, Wang D, Shi SR, Zhang T, et al. Nanoscaled red blood cells facilitate breast cancer treatment by combining photothermal/photodynamic therapy and chemotherapy. *Biomaterials* 2018;**155**:25–40.
4. Zhu DW, Fan F, Huang CL, Zhang ZM, Qin Y, Lu L, et al. Bubble-generating polymersomes loaded with both indocyanine green and doxorubicin for effective chemotherapy combined with photothermal therapy. *Acta Biomater* 2018;**75**:386–97.
5. Xu WJ, Qian JM, Hou GH, Suo AL, Wang YP, Wang JL, et al. Hyaluronic acid-functionalized gold nanorods with pH/NIR dual responsive drug release for synergetic targeted photothermal chemotherapy of breast cancer. *ACS Appl Mater Interfaces* 2017;**9**:36533–47.
6. Liu R, Hu C, Yang YY, Zhang JQ, Gao HL. Theranostic nanoparticles with tumor-specific enzyme-triggered size reduction and drug release to perform photothermal therapy for breast cancer treatment. *Acta Pharm Sin B* 2019;**9**:410–20.

7. Hirsch LR, Stafford RJ, Bankson JA, Sershen SR, Rivera B, Price RE, et al. Nanoshell-mediated near-infrared thermal therapy of tumors under magnetic resonance guidance. *Proc Natl Acad Sci U S A* 2003; **100**:13549−54.
8. Carpin LB, Bickford LR, Agollah G, Yu TK, Schiff R, Li Y, et al. Immunoconjugated gold nanoshell-mediated photothermal ablation of trastuzumab-resistant breast cancer cells. *Breast Canc Res Treat* 2011; **125**:27−34.
9. Chen JY, Wang DL, Xi JF, Au L, Siekkinen A, Warsen A, et al. Immuno gold nanocages with tailored optical properties for targeted photothermal destruction of cancer cells. *Nano Lett* 2007;**7**:1318−22.
10. Chen JY, Glaus C, Laforest R, Zhang Q, Yang MX, Gidding M, et al. Gold nanocages as photothermal transducers for cancer treatment. *Small* 2010;**6**:811−7.
11. Gao L, Fei JB, Zhao J, Li H, Cui Y, Li JB. Hypocrellin-loaded gold nanocages with high two-photon efficiency for photothermal/photodynamic cancer therapy *in vitro*. *ACS Nano* 2012;**6**: 8030−40.
12. Piao JG, Wang LM, Gao F, You YZ, Xiong YJ, Yang LH. Erythrocyte membrane is an alternative coating to polyethylene glycol for prolonging the circulation lifetime of gold nanocages for photothermal therapy. *ACS Nano* 2014;**8**:10414−25.
13. Huang XH, El-Sayed IH, Qian W, El-Sayed MA. Cancer cell imaging and photothermal therapy in the near-infrared region by using gold nanorods. *J Am Chem Soc* 2006;**128**:2115−20.
14. Huang XH, Jain PK, El-Sayed IH, El-Sayed MA. Plasmonic photothermal therapy (PPTT) using gold nanoparticles. *Laser Med Sci* 2008; **23**:217−28.
15. Tsai MF, Chang SHG, Cheng FY, Shanmugam V, Cheng YS, Su CH, et al. Au nanorod design as light-absorber in the first and second biological near-infrared windows for *in vivo* photothermal therapy. *ACS Nano* 2013;**7**:5330−42.
16. Dickerson EB, Dreaden EC, Huang XH, El-Sayed IH, Chu HH, Pushpanketh S, et al. Gold nanorod assisted near-infrared plasmonic photothermal therapy (PPTT) of squamous cell carcinoma in mice. *Canc Lett* 2008;**269**:57−66.
17. Park JH, von Maltzahn G, Xu MJ, Fogal V, Kotamraju VR, Ruoslahti E, et al. Cooperative nanomaterial system to sensitize, target, and treat tumors. *Proc Natl Acad Sci U S A* 2010;**107**:981−6.
18. Li DD, Zhang M, Xu F, Chen YZ, Chen BF, Chang Y, et al. Biomimetic albumin-modified gold nanorods for photothermo-chemotherapy and macrophage polarization modulation. *Acta Pharm Sin B* 2018;**8**:74−84.
19. Kam NWS, O'Connell M, Wisdom JA, Dai HJ. Carbon nanotubes as multifunctional biological transporters and near-infrared agents for selective cancer cell destruction. *Proc Natl Acad Sci U S A* 2005;**102**: 11600−5.
20. Moon HK, Lee SH, Choi HC. *In vivo* near-infrared mediated tumor destruction by photothermal effect of carbon nanotubes. *ACS Nano* 2009;**3**:3707−13.
21. Robinson JT, Welsher K, Tabakman SM, Sherlock SP, Wang HL, Luong R, et al. High performance *in vivo* near-IR (> 1 μm) imaging and photothermal cancer therapy with carbon nanotubes. *Nano Res* 2010;**3**:779−93.
22. Liang C, Diao S, Wang C, Gong H, Liu T, Hong GS, et al. Tumor metastasis inhibition by imaging-guided photothermal therapy with single-walled carbon nanotubes. *Adv Mater* 2014;**26**:5646.
23. Yang K, Zhang SA, Zhang GX, Sun XM, Lee ST, Liu ZA. Graphene in mice: ultrahigh *in vivo* tumor uptake and efficient photothermal therapy. *Nano Lett* 2010;**10**:3318−23.
24. Robinson JT, Tabakman SM, Liang YY, Wang HL, Casalongue HS, Daniel V, et al. Ultrasmall reduced graphene oxide with high near-infrared absorbance for photothermal therapy. *J Am Chem Soc* 2011; **133**:6825−31.
25. Gao HC, Sun YM, Zhou JJ, Xu R, Duan HW. Mussel-inspired synthesis of polydopamine-functionalized graphene hydrogel as reusable adsorbents for water purification. *ACS Appl Mater Interfaces* 2013;**5**: 425−32.
26. Markovic ZM, Harhaji-Trajkovic LM, Todorovic-Markovic BM, Kepic DP, Arsikin KM, Jovanovic SP, et al. *In vitro* comparison of the photothermal anticancer activity of graphene nanoparticles and carbon nanotubes. *Biomaterials* 2011;**32**:1121−9.
27. Xu LG, Cheng L, Wang C, Peng R, Liu Z. Conjugated polymers for photothermal therapy of cancer. *Polym Chem* 2014;**5**:1573−80.
28. Piao JG, Gao F, Yang LH. Acid-responsive therapeutic polymer for prolonging nanoparticle circulation lifetime and destroying drug-resistant tumors. *ACS Appl Mater Interfaces* 2016;**8**:936−44.
29. Yang K, Xu H, Cheng L, Sun CY, Wang J, Liu Z. *In vitro* and *in vivo* near-infrared photothermal therapy of cancer using polypyrrole organic nanoparticles. *Adv Mater* 2012;**24**:5586−92.
30. Cheng L, Yang K, Chen Q, Liu Z. Organic stealth nanoparticles for highly effective *in vivo* near-infrared photothermal therapy of cancer. *ACS Nano* 2012;**6**:5605−13.
31. Wang C, Xu H, Liang C, Liu YM, Li ZW, Yang GB, et al. Iron oxide@ polypyrrole nanoparticles as a multifunctional drug carrier for remotely controlled cancer therapy with synergistic antitumor effect. *ACS Nano* 2013;**7**:6782−95.
32. Zheng MB, Yue CX, Ma YF, Gong P, Zhao PF, Zheng CF, et al. Single-step assembly of DOX/ICG loaded lipid-polymer nanoparticles for highly effective chemo-photothermal combination therapy. *ACS Nano* 2013;**7**:2056−67.
33. Srinivasan S, Manchanda R, Lei TJ, Nagesetti A, Fernandez-Fernandez A, McGoron AJ. Targeted nanoparticles for simultaneous delivery of chemotherapeutic and hyperthermia agents—an *in vitro* study. *J Photochem Photobiol B Biol* 2014;**136**:81−90.
34. Hui LW, Qin S, Yang LH. Upper critical solution temperature polymer, photothermal agent, and erythrocyte membrane coating: an unexplored recipe for making drug carriers with spatiotemporally controlled cargo release. *ACS Biomater Sci Eng* 2016;**2**:2127−32.
35. Dong K, Liu Z, Li ZH, Ren JS, Qu XG. Hydrophobic anticancer drug delivery by a 980 nm laser-driven photothermal vehicle for efficient synergistic therapy of cancer cells *in vivo*. *Adv Mater* 2013;**25**: 4452−8.
36. Peng SW, He YY, Er M, Sheng YZ, Gu YQ, Chen HY. Biocompatible CuS-based nanoplatforms for efficient photothermal therapy and chemotherapy *in vivo*. *Biomater Sci* 2017;**5**:475−84.
37. Sheng GP, Chen Y, Han LJ, Huang Y, Liu XL, Li LJ, et al. Encapsulation of indocyanine green into cell membrane capsules for photothermal cancer therapy. *Acta Biomater* 2016;**43**:251−61.
38. Huang W, Huang YY, You YY, Nie TQ, Chen TF. High-yield synthesis of multifunctional tellurium nanorods to achieve simultaneous chemo-photothermal combination cancer therapy. *Adv Funct Mater* 2017;**27**: 171388.
39. Su SS, Tian YH, Li YY, Ding YP, Ji TJ, Wu MY, et al. "Triple-punch" strategy for triple negative breast cancer therapy with minimized drug dosage and improved antitumor efficacy. *ACS Nano* 2015;**9**:1367−78.
40. Kelkar SS, Reineke TM. Theranostics: combining imaging and therapy. *Bioconjugate Chem* 2011;**22**:1879−903.
41. Shen S, Tang HY, Zhang XT, Ren JF, Pang ZQ, Wang DG, et al. Targeting mesoporous silica-encapsulated gold nanorods for chemo-photothermal therapy with near-infrared radiation. *Biomaterials* 2013;**34**:3150−8.
42. Xue X, Fang T, Yin LY, Jiang JQ, He YP, Dai YH, et al. Multistage delivery of CDs-DOX/ICG-loaded liposome for highly penetration and effective chemo-photothermal combination therapy. *Drug Deliv* 2018;**25**:1826−39.
43. Shi ZY, Chu CC, Zhang Y, Su ZJ, Lin HR, Pang X, et al. Self-assembled metal-organic nanoparticles for multimodal imaging-guided photothermal therapy of hepatocellular carcinoma. *J Biomed Nanotechnol* 2018;**14**:1934−43.
44. Yang Y, Liu JJ, Liang C, Feng LZ, Fu TT, Dong ZL, et al. Nanoscale metal-organic particles with rapid clearance for magnetic resonance imaging-guided photothermal therapy. *ACS Nano* 2016;**10**:2774−81.
45. Pei P, Yang F, Liu JX, Hu HR, Du XY, Hanagata N, et al. Composite-dissolving microneedle patches for chemotherapy and photothermal therapy in superficial tumor treatment. *Biomater Sci* 2018;**6**:1414−23.

46. Yu WQ, Liu R, Zhou Y, Gao HL. Size-tunable strategies for a tumor targeted drug delivery system. *ACS Cent Sci* 2020;**6**:100−16.
47. Wang S, Huang P, Chen XY. Hierarchical targeting strategy for enhanced tumor tissue accumulation/retention and cellular internalization. *Adv Mater* 2016;**28**:7340−64.
48. Guo Q, He X, Li C, He YQ, Peng YY, Zhang Y, et al. Dandelion-like tailorable nanoparticles for tumor microenvironment modulation. *Adv Sci* 2019;**6**:1901430.
49. Chen BL, Dai WB, He B, Zhang H, Wang XQ, Wang YG, et al. Current multistage drug delivery systems based on the tumor microenvironment. *Theranostics* 2017;**7**:538−58.
50. Su YL, Yu TW, Chiang WH, Chiu HC, Chang CH, Chiang CS, et al. Hierarchically targeted and penetrated delivery of drugs to tumors by size-changeable graphene quantum dot nanoaircrafts for photolytic therapy. *Adv Funct Mater* 2017;**27**:1700056.
51. Xu JH, Gao FP, Li LL, Ma HL, Fan YS, Liu W, et al. Gelatin-mesoporous silica nanoparticles as matrix metalloproteinases-degradable drug delivery systems *in vivo*. *Microporous Mesoporous Mater* 2013;**182**:165−72.
52. Agheb M, Dinari M, Rafienia M, Salehi H. Novel electrospun nanofibers of modified gelatin-tyrosine in cartilage tissue engineering. *Mater Sci Eng C-Mater Biol Appl* 2017;**71**:240−51.
53. Xu Y, Zhang JN, Liu XY, Huo PC, Zhang Y, Chen H, et al. MMP-2-responsive gelatin nanoparticles for synergistic tumor therapy. *Pharmaceut Dev Technol* 2019;**24**:1002−13.
54. Ishikawa H, Nakamura Y, Jo J-i, Tabata Y. Gelatin nanospheres incorporating siRNA for controlled intracellular release. *Biomaterials* 2012;**33**:9097−104.
55. Pal A, Bajpai AK, Bajpai J. Study on facile designing, swelling properties and structural relationship of gelatin nanoparticles. *J Macromol Sci, Pure Appl Chem* 2019;**56**:206−14.
56. Calixto S, Ganzherli N, Gulyaev S, Figueroa-Gerstenmaier S. Gelatin as a photosensitive material. *Molecules* 2018;**23**:2064.
57. Satapathy MK, Nyambat B, Chiang CW, Chen CH, Wong PC, Ho PH, et al. A gelatin hydrogel-containing nano-organic PEI-Ppy with a photothermal responsive effect for tissue engineering applications. *Molecules* 2018;**23**:1256.
58. Zou Z, He XX, He DG, Wang KM, Qing ZH, Yang X, et al. Programmed packaging of mesoporous silica nanocarriers for matrix metalloprotease 2-triggered tumor targeting and release. *Biomaterials* 2015;**58**:35−45.
59. Hu GL, Zhang HQ, Zhang L, Ruan SB, He Q, Gao HL. Integrin-mediated active tumor targeting and tumor microenvironment response dendrimer-gelatin nanoparticles for drug delivery and tumor treatment. *Int J Pharm* 2015;**496**:1057−68.
60. Hu GL, Chun XL, Wang Y, He Q, Gao HL. Peptide mediated active targeting and intelligent particle size reduction-mediated enhanced penetrating of fabricated nanoparticles for triple-negative breast cancer treatment. *Oncotarget* 2015;**6**:41258−74.
61. Ruan SB, He Q, Gao HL. Matrix metalloproteinase triggered size-shrinkable gelatin-gold fabricated nanoparticles for tumor microenvironment sensitive penetration and diagnosis of glioma. *Nanoscale* 2015;**7**:9487−96.
62. Reddy N, Reddy R, Jiang QR. Crosslinking biopolymers for biomedical applications. *Trends Biotechnol* 2015;**33**:362−9.
63. Loth T, Hoetzel R, Kascholke C, Anderegg U, Schulz-Siegmund M, Hacker MC. Gelatin-based biomaterial engineering with anhydride-containing oligomeric cross-linkers. *Biomacromolecules* 2014;**15**:2104−18.
64. Carvalho JA, Abreu AS, Porto Ferreira VT, Goncalves EP, Tedesco AC, Pinto JG, et al. Preparation of gelatin nanoparticles by two step desolvation method for application in photodynamic therapy. *J Biomater Sci Polym Ed* 2018;**29**:1287−301.
65. Jaque D, Martinez Maestro L, del Rosal B, Haro-Gonzalez P, Benayas A, Plaza JL, et al. Nanoparticles for photothermal therapies. *Nanoscale* 2014;**6**:9494−530.
66. Qiao CD, Cao XL, FeiWang. Swelling behavior study of physically cross linked gelatin hydrogels. *Polym Polym Compos* 2012;**20**:53−7.
67. Zhang Y, Xu J. Mesoporous silica nanoparticle-based intelligent drug delivery system for bienzyme-responsive tumour targeting and controlled release. *R Soc Open Sci* 2018;**5**:170986.
68. Oryan A, Kamali A, Moshiri A, Baharvand H, Daemi H. Chemical crosslinking of biopolymeric scaffolds: current knowledge and future directions of crosslinked engineered bone scaffolds. *Int J Biol Macromol* 2018;**107**:678−88.
69. Sherlock SP, Tabakman SM, Xie LM, Dai HJ. Photothermally enhanced drug delivery by ultrasmall multifunctional FeCo/graphitic shell nanocrystals. *ACS Nano* 2011;**5**:1505−12.
70. Zhang LH, Qin Y, Zhang ZM, Fan F, Huang CL, Lu L, et al. Dual pH/reduction-responsive hybrid polymeric micelles for targeted chemo-photothermal combination therapy. *Acta Biomater* 2018;**75**:371−85.
71. Liu T, Choi H, Zhou R, Chen IW. RES blockade: a strategy for boosting efficiency of nanoparticle drug. *Nano Today* 2015;**10**:11−21.
72. Xiong ZJ, Shen MW, Shi XY. Zwitterionic modification of nanomaterials for improved diagnosis of cancer cells. *Bioconjugate Chem* 2019;**30**:2519−27.
73. Liao JF, Li WT, Peng JR, Yang Q, Li H, Wei YQ, et al. Combined cancer photothermal-chemotherapy based on doxorubicin/gold nanorod-loaded polymersomes. *Theranostics* 2015;**5**:345−56.